PHYSICAL REVIEW B **78**, 094428 (2008)

Simple tight-binding theory for magnetoresistance in perfect sandwiched structures

H. G. Silva[1,2] and Y. G. Pogorelov[1]

[1]*IFIMUP, Universidade do Porto, R. Campo Alegre, 687, Porto 4169-007, Portugal*

[2]*CEOT, Universidade do Algarve, Campus de Gambelas, Faro 8005-139, Portugal*

(Received 20 February 2008; revised manuscript received 11 April 2008; published 30 September 2008)

Recent fabrication of atomic precision nanodevices for spintronics greatly boosted their performance and also revealed interesting features as oscillating magnetoresistance with a number of atomic layers in a multilayered structure. This motivates the need to go beyond the usual theoretical approach of semiclassical continuous layers. Here the simple tight-binding dynamics is used to describe quantum conduction in a multicomponent system with spin-polarized electrodes separated by an ultrathin and atomically coherent nonmagnetic spacer (either metallic or insulating). A possibility is indicated for obtaining a huge resonant enhancement of magnetoresistance in such device by a special choice of gate voltage on the spacer element.

DOI: 10.1103/PhysRevB.78.094428 PACS number(s): 34.80.Pa, 73.50.−h, 73.61.−r, 75.70.Cn

I. INTRODUCTION

In our information-based society, the development of ultrahigh-density storage technology is a demanding priority. In this context, the necessity in ultrahigh sensitivity read-head devices is a great challenge from both theoretical and experimental points of view. Presently the most promising candidates for this purpose are the magnetic tunnel junctions (MTJs) made by two magnetic electrodes and separated by an ultrathin nonmagnetic spacer and their study becomes one of the central topics in the fast developing field of spintronics. Since the early studies by Tedrow and Meservey[1] on spin-polarized tunnel conduction, an impressive progress was achieved either in experiment[2–4] or in theory[5–7] for the spintronic applications of this mechanism. The most important recent advances are related to nanofabrication of multilayered systems on atomic precision level,[8,9] which raises the MTJ performance up to 400% of magnetoresistance and enables a breakthrough to their fundamental quantum properties. It should be noted that the overall number of electronic degrees of freedom in a device such as MTJ is macroscopically big, which generally suggests a quasiclassical behavior controlled by the spin-dependent relaxation times or by the spin-dependent tunneling amplitudes. However, the essential quantum behavior turns out to be possible at the effective separation of a small number (few units) of electronic degrees of freedom among the macroscopically big total number, e.g., the hoppings between the planes in the spacer among all possible hoppings in a junction, forming a partial quantization of energy spectrum and drastically enhancing the sensitivity of tunnel (or ballistic) transport to external factors.[10] Another natural quantization effect is the oscillatory behavior of conductance as a function either of the spacer thickness (or, more exactly, the number of atomic planes) or of electric field on the junction,[11] which may also allow an interesting possibility for specific magnetoconductance oscillations. All these need that the mode mixing due to the interface roughness and intraspacer defects be below the characteristic energy quantization scale and practically requires that the spacer consist of few atomic planes, coherent enough.

Consequently, the theoretical analysis of such systems requires a fully quantum-mechanical description rather than more traditional semiclassical approaches.[12,13] Up to the moment, there already exists a rather well-elaborated theoretical base for this description using the Green's function formalism and rigorous *ab initio* band calculations[14–16] as inputs to the general Kubo's formula. However, in many practical cases the direct use of the corresponding algorithms leads to heavy enough numerical work, specific for each particular configuration and not very well suited for qualitative predictions and optimization of device performance.

In this paper instead, the simple tight-binding dynamics in single-band approximation is developed using the straightforward equations of motion for on-site quantum-mechanical amplitudes to get a handy description of quantum magnetotransport in the ballistic regime (absence of either thermal or impurity scattering) for a trilayer system of spin-polarized electrodes with an ultrathin and atomically coherent nonmagnetic spacer. The motivation for our approach is an easy generalization to more promising device geometries (double barriers or double junctions, etc.) and conduction regimes (including finite electric-field effect) which will be presented in a forthcoming work. This presentation is mainly limited to the basics of the method and to its most characteristic results. Thus in Sec. II the explicit quantum wave functions are obtained for the one-dimensional (1D) isolated atomic chain. In Sec. III the finite 1D chain is inserted between two 1D semi-infinite leads and the transmission and reflection coefficients for a collective electronic state are analytically calculated. Further, in Sec. VI this result is generalized to the three-dimensional (3D) case and the Landauer conductance formula[17] is used in the 3D version to yield a clear picture of basic quantum effects evolved in this coherent system. In Sec. V, the important effects of electronic correlation are included into consideration using the approximation of phenomenological interface potentials, which foresees a more consistent treatment in the spirit of density-functional theory (DFT). At last, in Sec. IV work summary and principal results are presented and commented.

II. BASIC CHAIN MODEL

The simplest model for transport over exact electronic states considers a linear chain of n identical atoms with

 ©2008 The American Physical Society

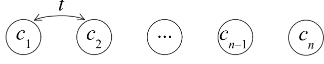

FIG. 1. Finite atomic chain with tight-binding amplitude t.

single available electronic state $|l\rangle$ on each lth atomic site and describes the single-electron dynamics in the simplest tight-binding approximation with (real) hopping amplitude t (Fig. 1) between nearest-neighbor sites (taking the distance between them as unit length). In this coupled chain, any collective electronic state can be expressed as $|c\rangle=\Sigma_{l=1}^{n}c_l|l\rangle$ with complex amplitudes c_l and atomic states $|l\rangle=\hat{c}_l^{\dagger}|0\rangle$, generated by the second quantization operators acting on the vacuum state $|0\rangle$. Choosing the on-site atomic energy as a reference ($\varepsilon_c=0$), we write the Hamiltonian operator as

$$\hat{H}^{(n)}=t\sum_{l=1}^{n-1}(\hat{c}_l^{\dagger}\hat{c}_{l+1}+\hat{c}_{l+1}^{\dagger}\hat{c}_l) \tag{1}$$

and obtain the electronic spectrum ε_m $(m=1,\ \ldots,n)$ as the roots of the secular equation $D_n(\varepsilon)=\det(\varepsilon-\hat{H}^{(n)})=0$ with the corresponding Hamiltonian matrix $H_{l,l'}^{(n)}=\langle l|\hat{H}^{(n)}|l'\rangle$ $=t(\delta_{l,l+1}\theta_{l-1}+\delta_{l,l-1}\theta_{n-l})$ (where $\delta_{l,l'}$ is the Kronecker delta and $\theta_l=1$ if $l>0$, otherwise zero). These determinants satisfy the recurrent relation,

$$D_n(\varepsilon)=\varepsilon D_{n-1}(\varepsilon)-t^2D_{n-2}(\varepsilon), \quad n\geq 2, \tag{2}$$

with the initial conditions $D_0(\varepsilon)=1,\quad D_1(\varepsilon)=\varepsilon$ that define them exactly through the second kind Chebyshev polynomials: $D_n(\varepsilon)=t^n u_n(\varepsilon/2t)$.[18] Then it is convenient to pass to these dimensionless polynomials $u_n(x)$ as functions of the dimensionless variable $x=\varepsilon/2t$ by rewriting Eq. (2) as

$$2xu_n(x)=u_{n+1}(x)+u_{n-1}(x), \tag{3}$$

with $u_0(x)=1,\quad u_1(x)=2x$. A useful trigonometric parametrization $u_l(\cos\theta)=\sin[(l+1)\theta]/\sin\theta$ permits us to present the general solution of Eq. (3) as

$$u_l(x)=\frac{\sin[(l+1)q_x]}{\sin q_x}, \tag{4}$$

where $q_x=\arccos x$. Then the discrete energy spectrum resulting from zeros of $u_n(x)$ is explicitly given by

$$\varepsilon_m=2t\cos\frac{\pi m}{n+1}, \quad m=1,\ \ldots,n. \tag{5}$$

Now let $c(x)=[c_1(x),\ \ldots,c_n(x)]$ be the eigenvector of the Hamiltonian matrix [Eq. (2)] related to the eigenenergy $\varepsilon=2tx$ (in what follows we mostly drop the explicit energy arguments of amplitudes like c_l). Its components satisfy the tight-binding equations of motion,

$$2xc_l=c_{l+1}+c_{l-1} \quad \text{for } 2\leq l\leq n-1, \tag{6}$$

completed by $2xc_1=c_2$ and $2xc_n=c_{n-1}$. Since Eq. (6) for c_l/c_1 is just equivalent to Eq. (3) for u_{l-1}, the eigenvector components can be written as

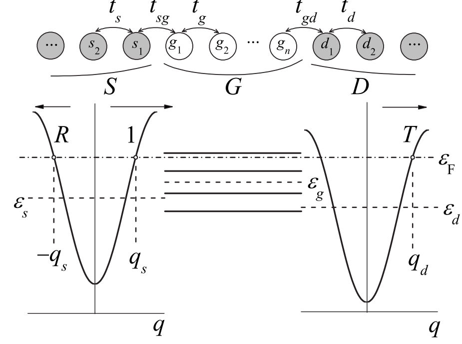

FIG. 2. Composite system of finite n chain (gate element, G) inserted between two semi-infinite chain leads (source, S, and drain, D). The energy diagram shows the on-site energy levels (dashed line) for ith element ($i=s,g,d$) and the Fermi level (dot-dashed line) whose crossings with the continuous S- and D-dispersion curves define the wave numbers for incoming (q_s), reflected ($-q_s$), and transmitted (q_d) parts of the Fermi state. Notice that the Fermi level generally does not match any of the discrete levels (solid) in the central (G) element.

$$c_l=\frac{\sin(lq_x)}{\sin q_x}c_1. \tag{7}$$

We notice that this solution also satisfies the above-mentioned equations of motion for c_1 and c_n and provides the “closed” boundary conditions,

$$c_0=c_{n+1}=0. \tag{8}$$

As usual, the value of c_1 is fixed by the normalization condition, $\Sigma_l|c_l(x)|^2=1$, giving finally the lth component of the eigenvector (related to the eigenenergy $\varepsilon_m=2tx_m$) as

$$c_l(x_m)=\sqrt{\frac{2}{n+1}}\sin\frac{\pi ml}{n+1}.$$

Our next purpose is to consider this finite chain inserted into the “circuit” between two semi-infinite chain leads.

III. TRANSMISSION THROUGH DISCRETE CHAIN STRUCTURE

For a composite system of finite n chain (in what follows called the gate, G) between two semi-infinite chain leads, S (source) and D (drain) (Fig. 2), the tight-binding Hamiltonian [Eq. (1)] is extended to $\hat{H}=\hat{h}^s+\hat{h}^d+\hat{h}^g+\hat{h}^{sg}+\hat{h}^{gd}$, where

$$\hat{h}^s=\sum_{l=1}^{\infty}[\varepsilon_s\hat{s}_l^{\dagger}\hat{s}_l+t_s(\hat{s}_l^{\dagger}\hat{s}_{l+1}+\text{H.c.})],$$

$$\hat{h}^g=\sum_{l=1}^{n}[\varepsilon_g\hat{g}_l^{\dagger}\hat{g}_l+t_g(\hat{g}_l^{\dagger}\hat{g}_{l+1}+\text{H.c.})],$$

$$\hat{h}^{sg}=t_{sg}(\hat{s}_1^{\dagger}\hat{g}_1+\text{H.c.}), \tag{9}$$

including the respective on-site energies ε_i $(i=s,d,g)$ and hopping parameters t_i $(i=s,sg,g,gd,d)$, while the operators

$\hat{h}^d$ and $\hat{h}^{gd}$ are analogous to $\hat{h}^s$ and $\hat{h}^{sg}$ with the formal change in indices $s \to d$. For this macroscopic system, the energy spectrum includes continuous S and D bands $\varepsilon_{i,q}=\varepsilon_i+2t_i \cos q$, $i=s,d$ and possibly discrete G levels outside these bands. The collective eigenstate for a given energy ε can be found from the equations of motion that generalize Eq. (6). We denote s_l, g_l, or d_l the respective local amplitudes of the wave function and define the dimensionless dynamical variables $x_i=(\varepsilon-\varepsilon_i)/2t_i$ $(i=s,g,d)$. Let the S amplitude be a sum of an incident wave of intensity 1 with the wave number $q_s=\arccos x_s$ and a reflected wave with certain amplitude R and the wave number $-q_s$,

$$s_l = e^{-iq_s l} + \mathrm{R}e^{iq_s l} \tag{10}$$

(for regressive order of sites l in S), and the D amplitude presents a transmitted wave with certain amplitude T and the wave number $q_d=\arccos x_d$,

$$d_l = Te^{iq_d l}. \tag{11}$$

Equations (10) and (11) refer to one of fundamental solutions for given ε (besides that where the incident and reflected waves belong to D and the transmitted one does to S). These forms automatically satisfy the equations of motion within S and D,

$$2x_s s_l = s_{l-1} + s_{l+1}, \quad 2x_d d_l = d_{l-1} + d_{l+1} \tag{12}$$

(for $l \geq 2$), while the pairs of equations on the S/G and G/D interfaces,

$$2s_1 \cos q_s = s_2 + \frac{t_{sg}}{t_s} g_1,$$

$$u_1 g_1 = g_2 + \frac{t_{sg}}{t_g} s_1, \tag{13}$$

and

$$2d_1 \cos q_d = d_2 + \frac{t_{gd}}{t_d} g_n,$$

$$u_1 g_n = g_{n-1} + \frac{t_{gd}}{t_g} d_1, \tag{14}$$

are the discrete analogs of the usual boundary conditions for continuous-wave function and its derivative.[19] They permit us to express the terminal pairs of G amplitudes through the asymptotic parameters R, T, q_s, and q_d,

$$g_1 = \frac{t_s}{t_{sg}}(1+R), \quad g_2 = \frac{t_s}{t_{sg}}[u_1 - \gamma_s^* + (u_1 - \gamma_s)R],$$

$$g_n = \frac{t_d}{t_{gd}} T, \quad g_{n-1} = \frac{t_d}{t_{gd}}(u_1 - \gamma_d)T, \tag{15}$$

with the interface parameters $\gamma_s=\mathrm{e}^{iq_s}t_{sg}^2/t_g t_s$ and $\gamma_d=e^{iq_d}t_{gd}^2/t_g t_d$. The polynomials $u_l \equiv u_l(x_g)$ are formally the same as given by Eq. (4) with the energy argument $x_g=(\varepsilon-\varepsilon_g)/2t_g$. However, the energies ε of our main interest for the transport processes are those close to the Fermi energy ε_F which is generally *not* an eigenvalue [Eq. (5)] for the isolated G element. Therefore the transient "momentum" $q_g=\arccos x_g$ (not necessarily real) breaks down the closed boundary conditions [Eq. (8)] for G and thus enables continuity of quantum states along the composite system. Next, using Eq. (6) for this element in the form

$$u_1 g_l = g_{l+1} + g_{l-1}, \tag{16}$$

it is possible to inter-relate the terminal G amplitudes,

$$g_{n-1} = u_{n-2} g_1 - \frac{t_{sg}}{t_g} u_{n-3} s_1,$$

$$g_n = u_{n-1} g_1 - \frac{t_{sg}}{t_g} u_{n-2} s_1. \tag{17}$$

Then, Eqs. (15) and (17) yield two independent relations between the coefficients R and T. Those are readily solved to give

$$R(x_s,x_g,x_d) = -\frac{\bar{D}_n}{D_n},$$

$$T(x_s,x_g,x_d) = -2i\frac{t_{sg}\,t_{gd}}{t_g t_d}\frac{\sin q_s}{D_n}, \tag{18}$$

where the resonance properties result from the denominator,

$$D_n(x_s,x_g,x_d) = u_n - (\gamma_s + \gamma_g)u_{n-1} + \gamma_s\gamma_d u_{n-2}, \tag{19}$$

with the relevant variables $x_i=(\varepsilon-\varepsilon_i)/2t_i$ as arguments of complex factors γ_i and real polynomials u_l, and $\bar{D}_n(x_s,x_g,x_d) \equiv D_n(x_s+\pi,x_g,x_d)$. Since, in the considered 1D case, all $x_i(\varepsilon)=(\varepsilon-\varepsilon_i)/2t_i$ are defined by the single energy variable ε, the coefficients R and T can be also defined as functions of energy: $R(\varepsilon) \equiv R[x_s(\varepsilon),x_g(\varepsilon),x_d(\varepsilon)]$ and $T(\varepsilon) \equiv T[x_s(\varepsilon),x_g(\varepsilon),x_d(\varepsilon)]$. It is important to notice that the result of Eqs. (18) and (19) is just analogous to that obtained with the Green's function techniques,[7] the factors γ_s and γ_d playing the role of interface Green's functions of Ref. 7. A typical behavior of the transmission coefficient $|T(\varepsilon)|^2$ is presented in Fig. 3. It shows n transmission resonances generated by n discrete energy levels of the G element (by n atoms in the chain) as they are passing over the Fermi level within the mutually displaced energy bands. The displacement can be due, for instance, to the Stoner splitting between majority and minority subbands of oppositely polarized S and D elements (see also Sec. VI). Notice that the resonances become sharper as the levels approach the band edges, and the maximum transmission in the asymmetric S-D band configuration is not limited to unity (the flux conservation does not mean the density conservation if the in- and out-velocities are not equal). This coefficient enters the Landauer formula[17] for the ballistic conductance through the 1D composite system (in zero-temperature limit),

$$G = \frac{e^2}{h}|T(\varepsilon_F)|^2, \tag{20}$$

with the Fermi energy ε_F. Now, allowing the S and D chains to support spin-polarized subbands $\varepsilon_{i,q,\sigma}=\varepsilon_{i,\sigma}+2t_i \cos q$

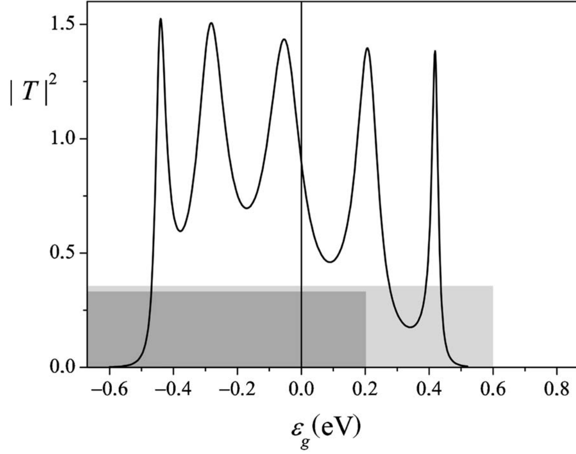

FIG. 3. Transmission coefficient $|T|^2$ as a function of the on-site energy ε_g in the gate element of the composite chain system for the choice of its parameters $\varepsilon_s=-0.4$ eV, $\varepsilon_d=-0.8$ eV (relative to the Fermi energy), $t_s=t_d=0.5$ eV, $t_g=t_{sg}=t_{gd}=0.25$ eV, and $n=5$. The shadowed areas indicate the (Stoner shifted) continuous bands, S (light gray) and D (dark gray).

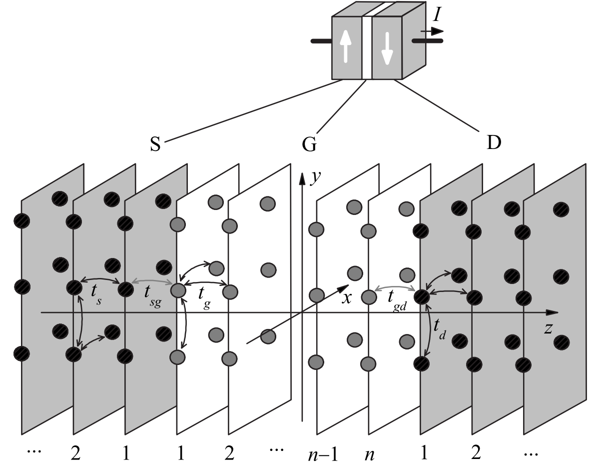

FIG. 4. Real multilayered structure where the current I flows through two ferromagnetic electrodes, S and D, separated by a non-magnetic spacer G and its model by the composite 3D system where a finite n-plane spacer is inserted between two semi-infinite leads.

(where $\varepsilon_{i,\sigma}=\varepsilon_i-\sigma\Delta_i$, $\sigma=\pm$ are the majority and minority-spin indices and Δ_i are the Stoner splitting parameters for $i=s,d$), we can introduce the energy and spin-dependent variables $x_{i,\sigma}(\varepsilon)=(\varepsilon-\varepsilon_{i,\sigma})/(2t_i)$, $i=s,d$, for in- and out-channels and obtain from Eq. (20) the spin-dependent conductance values $G_{\sigma,\sigma'}=(e^2/h)|T(x_{s,\sigma}(\varepsilon_F),x_{d,\sigma'}(\varepsilon_F),x_g(\varepsilon_F))|^2$. Finally, the (maximum) magnetoresistance (MR) is defined as usually through the difference between the conductance values $G_{\mathrm{P}}=G_{+,+}+G_{-,-}$ for parallel and $G_{\mathrm{AP}}=G_{+,-}+G_{+,-}$ for antiparallel S/D polarizations,

$$\mathrm{MR}=\frac{G_{\mathrm{P}}}{G_{\mathrm{AP}}}-1. \tag{21}$$

Although the state-of-the-art technology already permits development of such genuinely 1D devices[20] and the resonance behavior like that in Fig. 3 (different from the known quantized conductance steps versus voltage bias) can be directly sought in them, it is of major practical importance to generalize the above treatment for a more realistic multilayered structure and this will be done in Sec. IV.

IV. THREE-DIMENSIONAL MULTILAYERED STRUCTURE

Passing from 1D composite chain to multilayered (and spin-polarized) 3D lattice structure as shown in Fig. 4, we extend the indexing of site operators from $\hat{s}_l,\hat{d}_l$ and $\hat{g}_l$ to $\hat{s}_{l,\mathbf{m},\sigma},\hat{d}_{l,\mathbf{m},\sigma}$ and $\hat{g}_{l,\mathbf{m},\sigma}$, where $\mathbf{m}$ runs over N sites in the lth plane and σ is $\pm$. Our strategy in this case relies on the conservation of the transversal quasimomentum $\mathbf{k}=(k_x,k_y)$ in the transitions between the planes.[15,21] From the experimental point of view, this requires perfect interfaces that are only reachable with advanced molecular-beam epitaxy techniques.[22] To describe the situation where $\mathbf{k}$ is a good quantum number for independent 1D-like longitudinal transport channels, we pass from the site operators to the "planar wave" operators. Thus, for the lth plane in the S element, the latter operators are defined as

$$\hat{s}_{l,\mathbf{k},\sigma}=\frac{1}{\sqrt{N}}\sum_{\mathbf{m}}e^{ik\cdot\mathbf{m}}\hat{s}_{l,\mathbf{m},\sigma}, \tag{22}$$

and, similarly, the planar wave operators $\hat{d}_{l,\mathbf{k},\sigma}$ and $\hat{g}_{l,\mathbf{k},\sigma}$ for D and G elements are written. The related extension of the Hamiltonian is $\hat{H}=\sum_{\mathbf{k},\sigma}(\hat{h}^s_{\mathbf{k},\sigma}+\hat{h}^d_{\mathbf{k},\sigma}+\hat{h}^g_{\mathbf{k},\sigma}+\hat{h}^{sg}_{\mathbf{k},\sigma}+\hat{h}^{gd}_{\mathbf{k},\sigma})$, where the particular terms are analogous to those in Eq. (9) with the change in all the site operators by the planar wave ones and all the on-site energies ε_i by the transversal momentum subbands $\varepsilon_{i,k,\sigma}=\varepsilon_{i,\sigma}+2t_i(\cos k_x+\cos k_y)$, $i=s,d$, and $\varepsilon_{g,k,\sigma}=\varepsilon_g+2t_g(\cos k_x+\cos k_y)$. The equations of longitudinal motion in terms of the planar wave amplitudes $s_{l,\mathbf{k},\sigma}$, $d_{l,\mathbf{k},\sigma}$, and $g_{l,\mathbf{k},\sigma}$ (for given energy ε of the collective state) are obtained in analogy with the 1D case. Thus, in the leads S and D (beyond the interfaces, at $l>1$), they are analogs to Eq. (12),

$$2x_{s,\mathbf{k},\sigma}s_{l,\mathbf{k},\sigma}=s_{l-1,\mathbf{k},\sigma}+s_{l+1,\mathbf{k},\sigma},$$

$$2x_{d,\mathbf{k}}d_{l,\mathbf{k},\sigma}=d_{l-1,\mathbf{k},\sigma}+d_{l+1,\mathbf{k},\sigma}, \tag{23}$$

with $x_{i,\mathbf{k},\sigma}=(\varepsilon-\varepsilon_{i,\mathbf{k},\sigma})/(2t_i)$, $i=s,d$, while in the spacer G (at $1<l<n$), we have in analogy with Eqs. (7) and (15),

$$2x_{g,\mathbf{k}}g_{l,\mathbf{k},\sigma}=g_{l-1,\mathbf{k},\sigma}+g_{l+1,\mathbf{k},\sigma}, \tag{24}$$

with $x_{g,\mathbf{k}}=(\varepsilon-\varepsilon_{g,\mathbf{k}})/(2t_g)$. Also the equations for interface amplitudes,

$$2x_{s,\mathbf{k},\sigma}s_{\mathbf{k},1,\sigma}=s_{\mathbf{k},2,\sigma}+\frac{t_{sg}}{t_s}g_{\mathbf{k},1,\sigma},$$

$$2x_{g,\mathbf{k},\sigma}g_{\mathbf{k},1,\sigma}=g_{\mathbf{k},2,\sigma}+\frac{t_{sg}}{t_g}s_{\mathbf{k},1,\sigma},$$

$$2x_{g,\mathbf{k},\sigma}g_{\mathbf{k},n,\sigma} = g_{\mathbf{k},n-1,\sigma} + \frac{t_{gd}}{t_g}d_{\mathbf{k},1,\sigma},$$

$$2x_{d,\mathbf{k},\sigma}d_{\mathbf{k},1,\sigma} = d_{\mathbf{k},2,\sigma} + \frac{t_{gd}}{t_d}g_{\mathbf{k},1,\sigma}, \tag{25}$$

are analogous to Eqs. (13)–(15). The next derivation, in full similarity with the 1D case, leads to the full dispersion laws in the leads $\varepsilon_{i,\mathbf{k},q,\sigma}=\varepsilon_{i,\mathbf{k},\sigma}+2t_i \cos q$ (for $i=s,d$) and to the final conductance formula for particular in-out spin channels,

$$G_{\sigma\sigma'} = \frac{e^2}{h}\sum_{\mathbf{k}\in K}|T_{\sigma\sigma'}(\varepsilon_F,\mathbf{k})|^2. \tag{26}$$

Here the transmission coefficient depends on the relevant variables σ, σ', ε, and $\mathbf{k}$ according to $T_{\sigma\sigma'}(\varepsilon,\mathbf{k}) \equiv T(q_{s,\mathbf{k},\sigma},q_{g,\mathbf{k}},q_{d,\mathbf{k},\sigma'})$ with $q_{i,\mathbf{k},\sigma}=\arccos x_{i,\mathbf{k},\sigma}$ for $i=s,d$ and $q_{g,\mathbf{k}}=\arccos x_{g,\mathbf{k}}$, and the sum in $\mathbf{k}$ is restricted to the "permitted" range K, such that simultaneous equalities $\varepsilon_{s,\mathbf{k},q_s} =\varepsilon_{d,\mathbf{k},q_d}=\varepsilon_F$ result in certain *real* in- and out-momenta q_s and q_d. In more detail, the latter condition is expressed as

$$\begin{aligned}&\max\{-2,\max[x_{s,\sigma}(\varepsilon_F),x_{d,\sigma'}(\varepsilon_F)]-1\}\\ &\quad\le \cos k_x + \cos k_y\\ &\quad\le \min\{2,\min[x_{s,\sigma}(\varepsilon_F),x_{d,\sigma'}(\varepsilon_F)]+1\},\end{aligned} \tag{27}$$

fully defining the integration procedure (in the limit of continuous $\mathbf{k}$). It should be noted that the internal momentum q_g can be either real or imaginary in this course, depending on specific $\mathbf{k}$ in K. Therefore the attribution of purely "tunneling" or purely "metallic" conduction regime is here conventional to a certain extent, for instance, a predominant tunnel-like conductance can yield to metalliclike one with growing n_g. Then, seeking for optimum performance of the model MR device from Eq. (21), it is of interest to evaluate it as a function of the system parameters, mainly the number of atomic layers in the gate n and the on-site energy level of the gate ε_g (which can be possibly controlled through the gate bias). Also, variation of the latter parameter from positive to negative values permits to model in a unified way the passage from the tunnel magnetoresistance (TMR) to giant magnetoresistance (GMR) regime (in the above indicated sense).

The following numerical work can be oriented accordingly to some evident qualitative arguments. The variation of the integrand in Eq. (26) is mainly controlled by that of the polynomials $u_l(x_{g,\mathbf{k}})$ in the denominator of Eq. (19). As seen from the explicit equation (4), they are oscillating if $|x_{g,\mathbf{k}}| <1$ (that is, the sampling point $\varepsilon_{g,\mathbf{k}}$ in the G spectrum close enough to the Fermi energy ε_F) and exponentially growing if $|x_g|>1$ (remote enough $\varepsilon_{g,\mathbf{k}}$ from ε_F). Therefore, the conductance is generally expected to oscillate (either in ε_g or in n) as far as the level ε_g is close enough to ε_F (which can be compared to the GMR regime) and to exponentially decay at ε_g far enough from ε_F (a generalized TMR regime). The latter decay should asymptotically tend to $\mathrm{MR}(n)\propto\exp(-nx_{\min})$ with $x_{\min}=\min_{\mathbf{k}\in K}|x_{g,\mathbf{k}}|$ at $n\gg 1$.

In the latter case, the direct calculation by Eq. (21) may result in G_{P} and G_{AP} both exponentially small but the latter yet much smaller and thus in (arbitrarily) huge MR values.

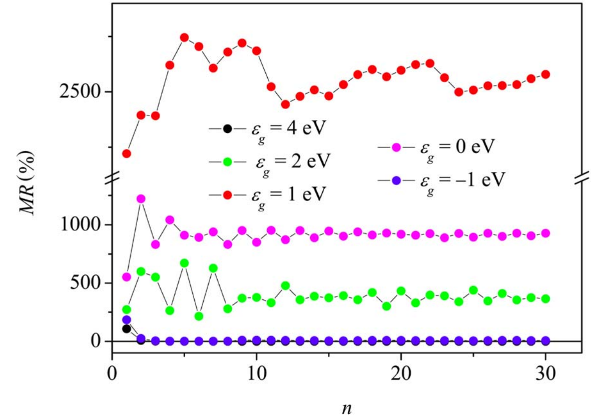

FIG. 5. (Color online) Magnetoresistance of a FM/NM/FM junction with the model parameters: $\varepsilon_{s,+}=\varepsilon_{d,+}=1.32$ eV, $\varepsilon_{s,-} =\varepsilon_{d,-}=3.36$ eV, $t_s=t_d=t_g=-0.6$ eV (like those from Ref. 25), and $\gamma_{s,d}=0.5$ as a function of the number n of spacer layers at fixed values of ε_g. Notice the exponential decay in the TMR-like regime either at the highest $\varepsilon_g=4$ eV or at the lowest $\varepsilon_g=-1$ eV and a strong enhancement with emergence of oscillatory behavior at intermediate ε_g (shallow-band regime).

However, they should not be physically attainable, taking into account that the real multiband electronic structure of transition metals always includes some additional conduction channels, for instance, due to the s bands, whose tunnel contribution slower decays than that of the d bands and is almost spin independent. Therefore it should dominate the transport in the indicated regime and make the real MR exponentially small. A simple phenomenological account of this mechanism in the considered single-band model can be done by introducing a certain spin-independent term G_0 into either G_{P} or G_{AP} values,

$$G_{\mathrm{P}} = G_{++} + G_{--} + G_0, \quad G_{\mathrm{AP}} = G_{+-} + G_{-+} + G_0, \tag{28}$$

to present the MR formula [Eq. (21), as

$$\mathrm{MR} = \frac{G_{++} + G_{--} - G_{+-} - G_{-+}}{G_{+-} + G_{-+} + G_0}. \tag{29}$$

It is just this formula that is used below for all practical MR calculations. Thus, using the band-structure parameters $\varepsilon_{s,+} =\varepsilon_{d,+}=1.32$ eV, $\varepsilon_{s,-}=\varepsilon_{d,-}=3.36$ eV, $t_s=t_d=t_g=-0.6$ eV, and $\gamma_{s,d}=0.5$ (a reasonable single-band fit for the real Fe band structure, see Refs. 23–25) and choosing for simplicity the constant value $G_0=0.1e^2/h$, we find that the MR behavior vs n indeed changes qualitatively at different choices of ε_g (Fig. 5). The TMR-like behavior with fast exponential decay appears either at high enough gate level, $\varepsilon_g \gtrsim 6t_g$ (which can be compared to a "positive" barrier in the continuum approximation), or at low enough gate level, $\varepsilon_g \lesssim -2t_g$ (a "negative" or "hole" barrier), but it develops GMR-like oscillations with greatly enhanced average MR amplitude at the intermediate ε_g values (which can be called the "shallow-band" regime). The oscillating behavior reveals similar types of periods that predicted in the Green's function treatment in Ref. 15, and it is in a qualitative agreement with that experimentally observed for MgO moderate tunnel bar-

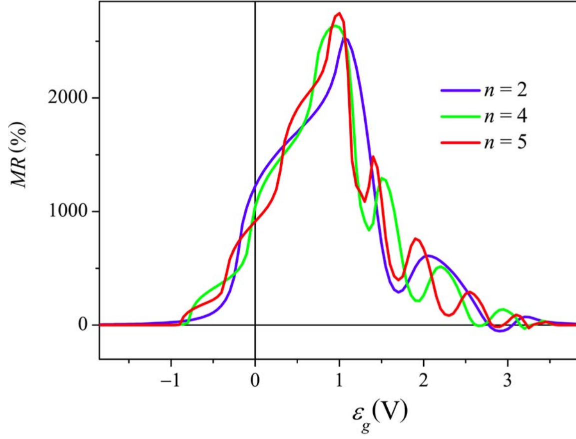

FIG. 6. (Color online) MR vs the on-site energy ε_g of the gate element for a junction with the same parameters as in Fig. 5 and various numbers of atomic planes in the gate element: n=2, n=4 and n=5. Compare the resonance peaks in the shallow-band regime with those in the 1D case of Fig. 3.

riers between Fe electrodes[8] except for stronger first oscillations. However, it will be shown below that these strong oscillations are effectively moderated when the specific interface effects between metal and insulator layers are taken into account. The most notable feature of the calculated MR is its amazingly high maximum value, of the order of 3000%, indicating a huge potentiality of the quantum coherent conduction regime.

For the same choice of parameters, the calculated dependencies of MR vs ε_g (at fixed values of n=2,4,5) are shown in Fig. 6. In concordance with the above considered MR(n) behavior, they practically vanish beyond the range of intermediate ε_g and display a finite number of resonance peaks within this range (reminiscent of n 1D resonances in Fig. 3), reaching the same highest order of magnitude in the shallow-band regime. These very high values in the present tight-binding approach contrast with the known result for the model of almost free electrons through the continuous rectangular barrier,[19] where MR reaches zero minimum at low barrier height. As yet, the MR(ε_g) dependence was only studied experimentally for Al-O spacers,[26] possessing most probably polycrystalline or amorphous structure and high enough ε_g, so it could be of interest to try it also with epitaxial MgO spacers and possibly with those spacer materials that can realize the shallow-band condition.

V. INTERFACIAL EFFECTS

In this section, we will discuss the interfacial effects present at the metal/insulator or metal/nonmagnetic-spacer interfaces. This is motivated by the analogy with the well-known case of Schottky barrier at metal/semiconductor interfaces, leading to such interesting physical effects as band bending.[27] It is known from x-ray and ultraviolet photoemission spectroscopies that some charge-transfer effects also appear at the metal-insulator interface, leading to the formation of an interfacial charge-dipole whose magnitude is defined by the localized states at interfaces.[28] Since this dipole directly affects the efficiency of tunneling, it is also important to evaluate its effect in the magnetoresistance.

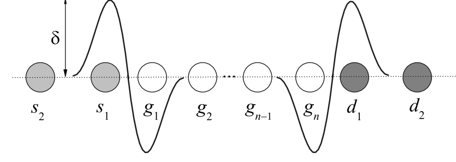

FIG. 7. Schematic representation of the interface charge energy, δ, created by a charge accumulation in the S/G and G/D interfaces, as a simplified description of the true self-consistent behavior.

The best treatment of this problem is to introduce self-consistently a charging energy (δ, commonly called the built-up voltage) due to a charge accumulation in the framework of the DFT. This is going to be done in the future work, but at the moment we will develop simple analytic formulas to take into account these interfacial effects qualitatively. Despite its simplicity, the model can exemplify in which way the formation of charge dipoles[29,30] affects the magnetoresistance ratio.

We go on using the same model of Sec. VI but considering extra charge energies $\pm\delta$ on the sites pertaining to the two atomic planes on both sides of each interface (see Fig. 7) as an approximation for more realistic charge and potential distributions around interfaces, obtained by numerical DFT calculations.[14] The δ perturbation results in new boundary conditions and, as a consequence, in a new transmission coefficient. In this approximation, there is no changes in equations of motion within the particular elements (S, D, and G), but new pairs of equations appear at the S/G and G/D interfaces, involving the charge energy δ,

$$(2\cos q_s + \delta/t_s)s_1 = s_2 + (t_{sg}/t_s)g_1,$$

$$(x_g - \delta/t_g)g_1 = g_2 + (t_{sg}/t_g)s_1,$$

$$(2\cos q_b + \delta/t_d)d_1 = d_2 + (t_{gd}/t_d)g_n,$$

$$(x_g - \delta/t_g)g_n = g_{n-1} + (t_{gd}/t_g)d_1. \tag{30}$$

These boundary conditions allow us to recalculate two-terminal G amplitudes as a function of the parameters R,T,q_s,q_d. Interconnecting these terminal amplitudes leads to the transmission formula [Eq. (18)] but with the modified denominator $D_{n,\delta}$=$A_n-B_n+C_n$, where

$$A_n = \left(1+\frac{\delta}{t_d}e^{iq_d}\right)\left(1+\frac{\delta}{t_s}e^{iq_s}\right)\left[u_n - 2\frac{\delta}{t_g}u_{n-1} + \left(\frac{\delta}{t_g}\right)^2 u_{n-2}\right],$$

$$B_n = \left[\gamma_s\left(1+\frac{\delta}{t_d}e^{iq_d}\right) + \gamma_d\left(1+\frac{\delta}{t_s}e^{iq_s}\right)\right]\left(u_{n-1} - \frac{\delta}{t_g}u_{n-2}\right),$$

$$C_n = \gamma_s\gamma_d u_{n-2}. \tag{31}$$

It is easy to see that $D_{n,\delta}\to D_n$ in the limit of $\delta\to 0$.

The MR defined from Eqs. (29) and (31) as a function of the number n of gate atomic planes and of the gate voltage ε_g for the three values of the interface potential δ is presented in Figs. 8 and 9. The obtained softening of first oscillations

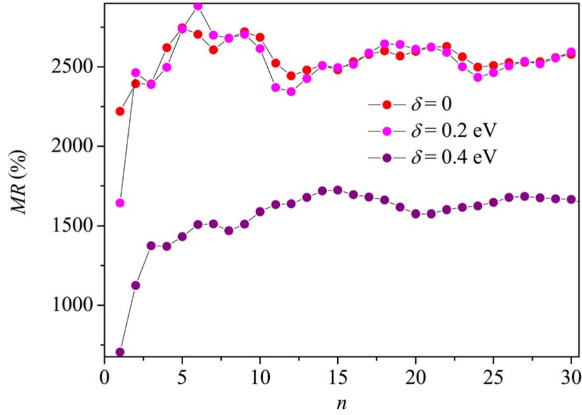

FIG. 8. (Color online) Effect of the interface charge energy on the MR(n) dependence. The system corresponds to the parameters as in Figs. 5 and 6 with $\varepsilon_g = 1$ eV and δ varying from 0 to 0.4 eV.

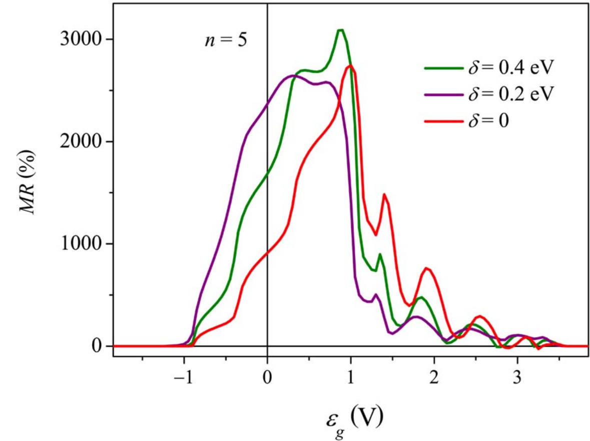

FIG. 9. (Color online) Effect of the interface charge energy on the MR(ε_g) dependence. The system corresponds to the parameters as in Figs. 5 and 6 with $n=5$ and δ varying from 0 to 0.4 eV.

makes these curves more similar to the experimental observations.[8] An unexpected result is that the effect of an extra barrier due to the charge energy can yet reinforce the calculated MR peak in the shallow-band regime, though reducing the values in the TMR regime at higher barrier height. Obviously, the charge energy barrier reduces the conductance (either in P or in AP configurations), but the MR enhancement is mainly due to a much stronger reduction in the AP conductance. Apparently it results from the wave-function localization caused by coherent resonances in the interfacial potential wells. This idea of charge energy induced resonances is corroborated by the calculated sharpening of peaks just in the AP conductance. Amazingly high peak MR values, reaching $\sim 3000\%$ for a reasonable choice of $\delta \sim 0.4$ eV (similar to the numerical estimate for Fe-MgO interfaces,[14]), should motivate the fabrication of new devices with the choice of such spacer materials as semiconducting (Ge, Si) or semimetalic (Sb, As). Though the peak value may be obviously decreased under the effects of electron-electron, electron-phonon, and electron-magnon interactions, finite temperature, and disorder, it expresses one of the principal results of this work, demonstrating that the highest possible MR value should be reached in the shallow-band regime for nonmagnetic spacer by adjusting to the strongest resonance condition, once electronic coherence is assured.

VI. CONCLUSIONS

In this work a theoretical approach was developed to fully coherent spin-dependent quantum transport in nanolayered magnetic junctions using single-band tight-binding model with explicit equations of motion for wave-function amplitudes. The analytic solutions for the transmission and reflection coefficients were generalized for a three-dimensional magnetic junction structure. The simple zero-temperature calculations have revealed the most pronounced enhancement of the magnetoresistance in the shallow-band regime, defined by low gate voltages (Fig. 6). Another important feature for this gate voltage regime is the calculated oscillatory behavior of MR with the number of atomic planes in the spacer. In support of these theoretical predictions, the calculations also reveal that the oscillatory regime starts already at moderate gate voltages, $\varepsilon_g \sim 2$ eV. This agrees rather well with the experimental observation by Yuasa *et al.*[8] of clear MR oscillations at low enough gate voltage barrier $\varepsilon_g \sim 0.4$ eV in a Co/MgO/Co structure. So it is concluded that the best MR values for a quantum magnetic junction could be reached using shallow-band materials for spacer layers, the possible candidates sought between transition metals [Cr (Ref. 31) in junctions of the type Fe/Cr/Fe or Zn in junctions of the type Co/Zn/Co], semiconductors (Ge, Si), or semimetals (Sb, As). Probably, the highest experimental value of TMR, $\sim 500\%$,[32] is due to going closer to this regime. Finally, the important effect of charge buildup (Sec. V) on the junction interface was also considered and, though in a simple phenomenological approach, a possibility is shown for even stronger enhancement of the magnetoresistance in the presence of the extra charge energy for the same shallow-band regime, emphasizing again the promise of using the low ε_g materials. To verify these model predictions, the future work must include various realistic effects, such as those of finite temperature and self-consistent DFT, to adopt also the multiband electronic structure, spin-transfer processes, and nonlinear conduction regimes.

ACKNOWLEDGMENTS

The authors wish to thank J. B. Sousa, P. P. Freitas, J. Lopes dos Santos, J. P. Araújo, and H. L. Gomes for their helpful discussions and friendly support of various aspects of this study. The work was partially supported by Portuguese Foundation of Science and Technology (FCT) through Grant No. SFRH/BD/24190/2005 (H.G.S.).

[1] P. M. Tedrow and R. Meservey, Phys. Rev. Lett. **26**, 192 (1971).
[2] Mary Beth Stearns, J. Magn. Magn. Mater. **5**, 167 (1977).
[3] R. Meservey, J. Appl. Phys. **49**, 1405 (1978).
[4] J. S. Moodera, L. R. Kinder, T. M. Wong, and R. Meservey, Phys. Rev. Lett. **74**, 3273 (1995).
[5] M. Büttiker, Phys. Rev. B **27**, 6178 (1983).
[6] K. M. Schep, P. J. Kelly, and G. E. W. Bauer, Phys. Rev. Lett. **74**, 586 (1995).
[7] J. Mathon, A. Umerski, and M. Villeret, Phys. Rev. B **55**, 14378 (1997).
[8] S. Yuasa, T. Nagahama, A. Fukushima, Y. Suzuki, and K. Ando, Nat. Mater. **3**, 868 (2004).
[9] S. S. P. Parkin, C. Kaiser, A. Panchula, P. M. Rice, B. Hughes, M. Samant, and S.-H. Yang, Nat. Mater. **3**, 862 (2004).
[10] J. J. Sun, R. C. Sousa, T. T. P. Galvão, V. Soares, and P. P. Freitas, J. Magn. Soc. Jpn. **23**, 55 (1999).
[11] S. Yuasa, T. Nagahama, T. Kawakami, K. Ando, and Y. Suzuki, J. Phys. D **35**, 2427 (2002).
[12] J. G. Simmons, J. Appl. Phys. **34**, 1793 (1963).
[13] M. Julliere, Phys. Lett. **54A**, 225 (1975).
[14] W. H. Butler, X.-G. Zhang, T. C. Schulthess, and J. M. MacLaren, Phys. Rev. B **63**, 054416 (2001).
[15] J. Mathon, M. Villeret, and H. Itoh, Phys. Rev. B **52**, R6983 (1995).
[16] J. Mathon and A. Umerski, Phys. Rev. B **63**, 220403(R) (2001).
[17] R. Landauer, IBM J. Res. Dev. **1**, 223 (1957).
[18] *Handbook of Mathematical Functions with Formulas, Graphs, and Mathematical Tables*, 9th ed., edited by M. Abramowitz and I. A. Stegun (Dover, New York, 1972).
[19] J. C. Slonczewski, Phys. Rev. B **39**, 6995 (1989).
[20] N. Agraït, A. Levy Yeyati, and J. M. van Ruitenbeeck, Phys. Rep. **377**, 81 (2003).
[21] H. Itoh, J. Phys. D **40**, 1228 (2007).
[22] S. Yuasa, A. Fukushima, H. Kubota, Y. Suzuki, and K. Ando, Appl. Phys. Lett. **89**, 042505 (2006).
[23] J. Callaway and C. S. Wang, Phys. Rev. B **16**, 2095 (1977).
[24] T. Nautiyal and S. Auluck, Phys. Rev. B **34**, 2299 (1986).
[25] On-line database of electronic structures available at https://caldb.nims.go.jp/
[26] N. Tezuka and T. J. Miyazaki, J. Magn. Magn. Mater. **177-181**, 1283 (1998).
[27] S. M. Sze, *Physics of Semiconctor Device* (Wiley, New York, 1981).
[28] M. Popinciuc, H. T. Jonkman, and B. J. van Wees, J. Appl. Phys. **101**, 093701 (2007).
[29] J. S. Moodera, J. Nowak, L. R. Kinder, P. M. Tedrow, R. J. M. van de Veerdonk, B. A. Smits, M. van Kampen, H. J. M. Swagten, and W. J. M. de Jonge, Phys. Rev. Lett. **83**, 3029 (1999).
[30] J. S. Moodera and J. Mathon, J. Magn. Magn. Mater. **200**, 248 (1999).
[31] F. Greullet, C. Tiusan, F. Montaigne, M. Hehn, D. Halley, O. Bengone, M. Bowen, and W. Weber, Phys. Rev. Lett. **99**, 187202 (2007).
[32] S. Yuasa and D. D. Djayaprawira, J. Phys. D **40**, R337 (2007).